
RESEARCH ARTICLE

Molecular Modeling of the HR2 and Transmembrane Domains of the SARS-CoV-2 S Protein in the Prefusion State

M. E. Bozdaganyan^{a,b} (ORCID: 0000-0003-1647-1627), P. S. Orekhov^{a,c} (ORCID: 0000-0003-4078-4762),
D. S. Litvinov^a, and V. N. Novoseletsky^{a,*} (ORCID: 0000-0003-4090-4859)

^a Biology Department, Moscow State University, Moscow, 119234 Russia

^b Semenov Federal Research Center for Chemical Physics, Russian Academy of Sciences, Moscow, 119991 Russia

^c Institute of Personalized Medicine, Sechenov University, Moscow, 119435 Russia

*e-mail: novoseletsky@mail.bio.msu.ru

Received May 25, 2021; revised June 22, 2021; accepted June 24, 2021

Abstract—SARS-CoV-2, the causative agent of COVID-19, remains the focus of research worldwide. SARS-CoV-2 entry into the cell starts with its S protein binding to the angiotensin-converting enzyme-2 (ACE2) expressed on the cell surface. The knowledge of the S protein's spatial structure is indispensable for understanding the molecular principles of its work. The S protein structure has been almost fully described using experimental approaches with the only exception for the protein's endodomain, the transmembrane domain, and the ectodomain parts adjacent to the latter. The paper reports molecular modelling of the S protein fragment corresponding to its coiled coil HR2 domain and fully palmitoylated transmembrane domain. Model stability in lipid bilayer was confirmed by all-atom and coarse-grained molecular dynamics simulations. It has been demonstrated that palmitoylation leads to a significant decrease in transmembrane domain mobility and local bilayer thickening, which may be relevant for protein trimerization.

Keywords: molecular modelling, SARS-CoV-2, S protein, lipid bilayer, palmitoylation, trimeric coiled coil

DOI: 10.3103/S0096392521030044

We are currently experiencing the third wave of the COVID-19 pandemics caused by SARS CoV-2. Huge effort is being made worldwide towards the development of vaccines and drugs that would aid in overcoming the worldwide COVID-19 crisis. The virus surface S protein, which plays the key role in virus entry into the host cell by binding human angiotensin-converting enzyme 2 (ACE2), is the main target of most vaccines.

The S protein consists of the two subunits S1 and S2, which are produced by the cleavage at the Arg685-Ser686 site carried by the cellular furin protease. The S1 subunit contains the signal peptide, N-terminal domain, and receptor-binding domain that interact with the ACE2 receptor. The S2 subunit encompasses the fusion peptide, heptad repeats 1 and 2 (HR1 and HR2), transmembrane domain (TMD), and endodomain. The full-size membrane S protein, whose spatial structure remains unresolved so far, forms a homotrimeric complex and facilitates the fusion of the host cell and virus particle membranes, and consequently, virus entry into the cell [1].

A large amount of structural data is currently available for the S protein ectodomain, the primary immune system target, whereas we have much less information about its TMD and proximal regions

localized close to the membrane [2]. It is assumed that the conformational mobility of the S protein is due to bending in a number of hinge regions, one of them being the region between HR2 and TMD [3]. Given that conformational mobility is crucial for the virus's entry into the cell and possibly plays a role in the accessibility of the S protein surface epitopes to antibodies, constructing an accurate model of the S protein fragment, including TMD and neighboring domains, is critically important.

In the present work, we have built a structural model of the S protein fragment containing TMD and the adjacent HR2 domain located at the outer membrane surface and endodomain fragment at the inner surface, including the cysteine-rich domain (cys) domain. We used all-atom and coarse-grained molecular dynamics (MD) simulations in a complex membrane to optimize the obtained model and assess the effects of cysteine palmitoylation on S protein mobility in the membrane and its local lipid environment.

MATERIALS AND METHODS

All-atom model assembly and parametrization. The structural model of the SARS CoV-2 S protein fragment (amino acid residues 1157–1256 encompassing

the HR2 domain, TMD, and cys domain) with the canonical sequence (Uniprot P0DTC2) was built using homology-based methods and two protein structures (PDB 2fxp [5] and 6e8w [6]) as templates with the aid of the Modeller software [4].

All-atom molecular dynamics protocol. The CHARMM-GUI web-server was used to preprocess the model before MD calculations [7] with palmitoylation of the cysteine residues 1235, 1236, 1241, 1242, 1244, 1248, 1249, 1251, 1254, 1255 (Fig. 1a). Membrane lipid composition was as described previously [8]: cholesterol : palmitoyl-sphingomyelin (PSM) : palmitoyl-oleoyl-phosphatidylethanolamine (POPE) : dipalmitoyl-phosphatidylethanolamine (DPPE) : palmitoyl-oleoyl-phosphatidylcholine (POPC) : palmitoyl-oleoyl-phosphatidylserine (POPS) : dipalmitoyl-phosphatidylcholine (DPPC) : dipalmitoyl-phosphatidylserine (DPPS) in a 15 : 10 : 9 : 6 : 3 : 3 : 2 : 2 ratio. The final ratio between lipid molecules after palmitoylation was 88 : 54 : 51 : 36 : 18 : 18 : 12 : 11, respectively. The total system size, including water molecules (TIP3P model) and Na⁺ and Cl⁻ ions (0.15 M), was 176 246 atoms. The cell size was 90 Å × 90 Å × 215 Å. System energy minimization and system equilibration was carried out according to the protocol recommended by the CHARMM-GUI web-server, which included the following steps: (1) system minimization using the steepest descend method, including 5000 steps, (2) six equilibration stages each 150–250 ps long with setting atoms velocities at the initial moment in accordance with the Maxwell distribution at 318 K and with gradual relaxation of the harmonic constraints on heavy atoms positions. MD was simulated using the Gromacs software [9] in the all-atom force field CHARMM36m [10] in the NPT ensemble at 318 K for 30 ns.

Coarse-grain model parametrization and coarse-grain molecular dynamics protocol. Initial models for coarse-grain MD calculations using the MARTINI 2.2 force field [11] were built using the martinize.py script based on the obtained all-atom model. A script available at <https://github.com/porekhov/palmitoylize> was used for protein palmitoylation. Molecular topology for the palmitoylated cysteine residue was obtained from the work previously published by the Tieleman group [12]. Palmitoylated and nonpalmitoylated trimer models were embedded into the model bilayer with the same composition as that used for the all-atom calculation and solvated (standard MARTINI field water model and Na⁺ and Cl⁻ ions in the concentration of 0.15 M were used) using the insane.py scenario (script). MD protocol was chosen in accordance with the recommendations provided by the Marrink group [13]. The simulations were made in the NPT ensemble at 318 K. The integration interval was set as 20 fs. The trajectories 1 μs in length were obtained for both systems. Gromacs 2019.4 was used to carry out the simulations as it was in the previous

case [9]. The g_lomepro software was used to calculate lipid bilayer thickness and lipid areas [14]. Python scripts implementing MDAnalysis libraries were used to calculate radial distribution functions.

RESULTS AND DISCUSSION

Model construction. The modelled S protein fragment contains several segments with differing degree of structural order (Fig. 1a). Modelling the HR2 domain is quite easy given the known structure of the same domain in the S protein of the closely related SARS-CoV coronavirus (100% identity for the residues 1157–1210) (PDB ID 2fxp, [5]). Monomer helices are oriented in such a way that the hydrophobic residues I1172, I1179, L1186, L1193, and L1200 are oriented towards the domain core.

At the same time, there are currently no high-identity templates available for the S protein TMD. For this reason, given the α-helical trimer structure and high number of aromatic residues present in the TMD N-terminus, we chose the human immunodeficiency virus (HIV) pg41 envelope protein TMD as a template (20% identity for the residues 1211–1240, with 33% identity for the residues 1211–1225 and 7% for the residues 1226–1240). Currently, a number of rather different structures have been obtained for this domain or one of its fragments (PDB ID 6e8w [6], 5jyn [15], and 6b3u [16]) making it difficult to choose one of them as a template. Furthermore, the conformation of the residues 1205–1210 still remains unresolved since the corresponding residues in the template are disordered. α-helix may be one of the possible conformations. In this case, the HR2 domain and TMD would form a coiled coil [3]. However, such conformation appears to be sterically unfavorable because the numerous aromatic residues in the S protein are located at all sides of the α-helices hindering coiled-coil formation. As a result, we chose the 6e8w template, notwithstanding it having a structure unusual for a TMD [6] with bending α-helices and long 3–10-helices. However, it was possible with this template to locate the bulk side chains of the aromatic residues without overlapping and disturbing the helical symmetry of the coiled coil. In this case, Y1209, I1216, G1223, V1230, and M1237 residues are found at the coiled coil axis. The SARS CoV-2 S protein TMD model obtained in this work (Fig. 1a; left) exhibited clear local similarity to the structure of the SARS-CoV S protein fragment (PDB ID 2run) obtained previously [17]. The deviation for the C atoms of the 11 central residues was not larger than 1 Å with most side chains having similar orientation.

Viral membrane protein palmitoylation has been studied for more than 40 years [18]. It is currently assumed that almost all cysteine residues in the C-terminal part of the S protein TMD and cys-domain of coronaviruses, including SARS-CoV, are palmitoylated [19]. For this reason, the choice of the plexin

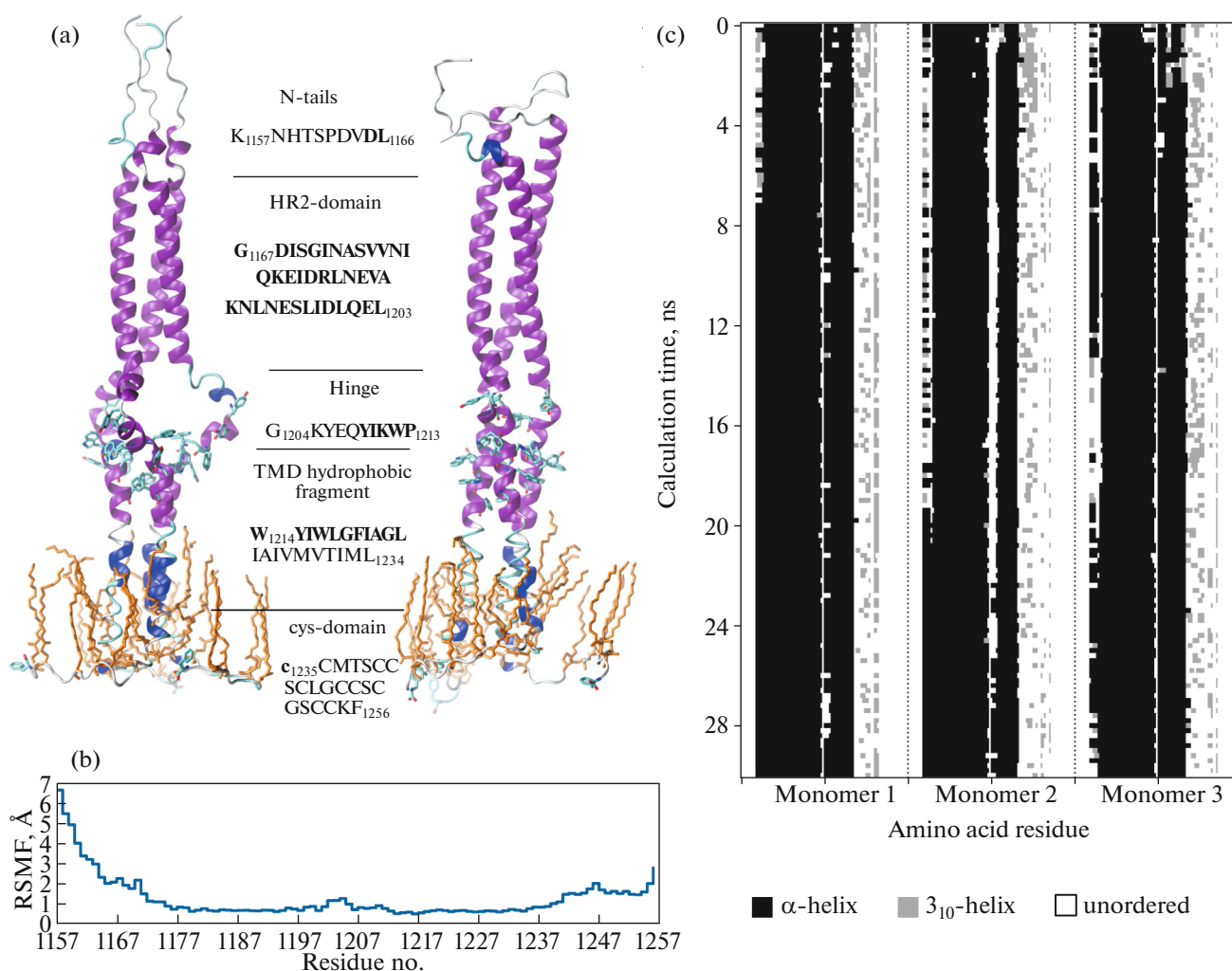


Fig. 1. (a) Structural model of the SARS CoV-2 S protein fragment (HR2 domain and TMD, residues 1157–1256) before (left) and after (right) molecular dynamics. α -Helices are indicated with violet, 3_{10} -helices with blue, and palmitoyl residues with orange. Aromatic residues are represented as sticks. (b) Root mean square fluctuation (RMSF) of the Ca-atoms of in the residues of the modeled S-protein fragment at the final stage of MD simulation (20–30 ns). (c) Changes in the secondary structure of the S-protein fragment during all-atom MD. Vertical axis—simulations time; horizontal axis—amino acid residues of the three monomers. Each dot in the plot shows the secondary of an individual residue at a certain moment of simulation.

structure (PDB ID 515k) also enriched in cysteine residues linked by a high number of disulfide bonds as a template for modelling SARS-CoV-2 S protein cys-domain structure made in Woo et al. (2020) [8] seems quite unreasonable. When building our model, we assumed all cysteine residues (ten in each subunit) to be palmitoylated. The final modelled structure is presented in Fig. 1a (left).

All-atom molecular dynamics. The CHARMM36m force field was chosen because of its being broadly used to study the dynamics of both proteins with low-ordered regions and protein–membrane systems [10]. Moreover, using this field allows one to more accurately reconstitute the conformation of experimentally determined structures, including short membrane proteins with non-ideal α -helical structure [20].

All-atom MD calculations showed that the structure of the studied protein undergoes some significant changes. It should be noted in this regard that, until the full structure of the protein is completely deciphered, the boundaries shown in Fig. 1a are, in a certain sense, tentative. For example, the TMHMM web service [21] predicts that the 1214–1234 residues (Fig. 1a) are located in the hydrophobic membrane layer. However, preliminary MD simulations showed that the location of bulk aromatic residues ($W_{1214}YIWLGF_{1220}$) in this membrane layer is sterically unfavorable, and, thus, this fragment “floats up” into the polar heads area of the outer lipid layer, simultaneously dragging some cys-domain residues from the polar heads area of the inner layer into the hydrophobic membrane layer. At the same time, it is known

that disordered secondary structure is untypical of the residues in the proteins' transmembrane fragments, which suggests the helical structure for the residues downstream L1234 as well. The structures of the monomer (PDB ID 6b3u [16]) and trimers (PDB ID 5jyn [15] and 6e8w [6]) of the HIV envelope protein gp41 TMD with the helix length of more than 30 residues also speak in favor of the elongated helical TMD. Based on this comparison, the helical fragment in our model can extend up to the C1241 residue, with the total length of each transmembrane helix being 34 residues.

In the course of MD simulations, the N-tails generally retained their disordered structure (Fig. 1a; right) and demonstrated high mobility (Fig. 1b). However, partial ordering of the N-terminal residues with the formation of α -helices could be observed (Fig. 1c), which is consistent with the helical conformation of the residues at the C-termini of several S protein ectodomain structures (PDB ID 6xr8, etc.). On the contrary, the coiled coil state of the HR2 domain appeared to be very stable, with highest mobility having been observed at its boundaries. The hinge fragment totally changed its conformation, with relatively slight thermal fluctuations of the atoms. The transmembrane domain generally retained its helical structure, including the conformationally strained 3–10-helices observed in the template (PDB ID 6e8w). Large fluctuations are not typically characteristic of transmembrane helices, with the model proposed in this paper being no exception. Finally, despite palmitoylation and close interaction with the membrane, the cys-domain showed rather high mobility on average, which was largely due to the relatively mobile closing K1256 and F1256 residues. Here, it should also be noted that palmitoyl residues attached to the C1235 and C1236 residues exhibited different behavior compared to those attached to the other cysteine residues. In our model, the indicated cysteine residues belong to TMDs and are visibly embedded into the membrane. This results in that the acyl chains attached to them are able, in terms of geometry, to penetrate into the membranes outer lipid layer, while the acyl chains of the remaining palmitoyl residues are incapable of doing so and fluctuate exclusively within the inner lipid layer. In this connection, it is interesting to note that mass spectrometry has previously shown [22] that cysteine residues at the C-terminus of the influenza A virus hemagglutinin TMD undergo not palmitoylation as such but rather stearylation. Our observations suggest that the position of cysteine residues at the C-terminus of the S-protein TMD also allows their stearylation, while the addition of a longer aliphatic chain will result in local disordering of the membrane environment. Thus, the MD results show that, under natural conditions, stearylation is the most likely posttranslational modification of the cysteine residues in the S-protein TMD.

Due to the presence of a weakly structured (at the initial moment) hinge, the HR2 domain can oscillate relative to the TMD, but the amplitude of these oscillations is relatively small. The angle between the domains changed insignificantly over the course of the trajectory, reaching 20° in the first 10 ns, decreasing to 5° as the hinge was structured over the next 10 ns, and remaining at this level thereafter.

It was interesting to compare the obtained results with the results of the NMR study of the S-protein TMD (residues 1209–1237) [23], whose amino acid sequence is different from the canonical one (Uniprot ID P0DTC2), namely, it contains Leu instead of Met in the positions 1229 and 1233 and Ser-Ser-Thr instead of Cys-Cys-Met in the positions 1235–1237. The authors were unsuccessful in determining the structure of the TMD N-terminal part (residues 1209–1217) enriched with aromatic residues, whereas the 1218–1237 residues formed a trimer consisting of nearly parallel α -helices, with the interhelical contacts being quite different from those in the previously studied trimers (PDB ID 5jyn, 6e8w, etc.) [23]. The authors found that the trimer core is made up of four nonpolar residues of similar size, namely, I1221, I1225, L1229, and L1233, which stabilize the trimer. However, this mutual position of the helices raises questions when we consider the canonical sequence, where two of these four residues are methionines and terminates with the Cys-Cys-Met tripeptide. First, larger methionine residues will disrupt the tight packing of the trimer core detected by NMR. Second, the overall geometry suggests that at least one cysteine residue in this pair (as well as one in the next C1240–C1241 pair) will also be oriented towards the core and its palmitoylation will, therefore, be hindered or at all impossible. Thus, the TMD model proposed on the basis of NMR analysis does not agree well with the native S-protein conformation.

We should also note that palmitoylation may possibly also contribute to maintaining the structural stability of the S protein TMD. As has already been mentioned above, a certain number of helices in TMD (Fig. 1a) are strained 3–10-helices, which are quite rare in membrane proteins. We performed a preliminary MD simulation for the nonpalmitoylated S-protein TMD. As a result, the 3–10-helices were transformed into the more stable α -helices, which disrupted the trimer structure (data not shown). In the case of MD stimulation for the palmitoylated TMD, no 3–10 transformation into α -helices was observed (Figs. 1a, 1c). Thus, we may state that palmitoylation reduces the conformational mobility of helices in the TMD and stabilizes its structure. An indirect confirmation of this palmitoylation function are the experimental data on the greater importance of palmitoylation of the cysteine residues located at the start of the cys-domain [24]. According to our model, these residues belong to TMD and their palmitoylation prevents

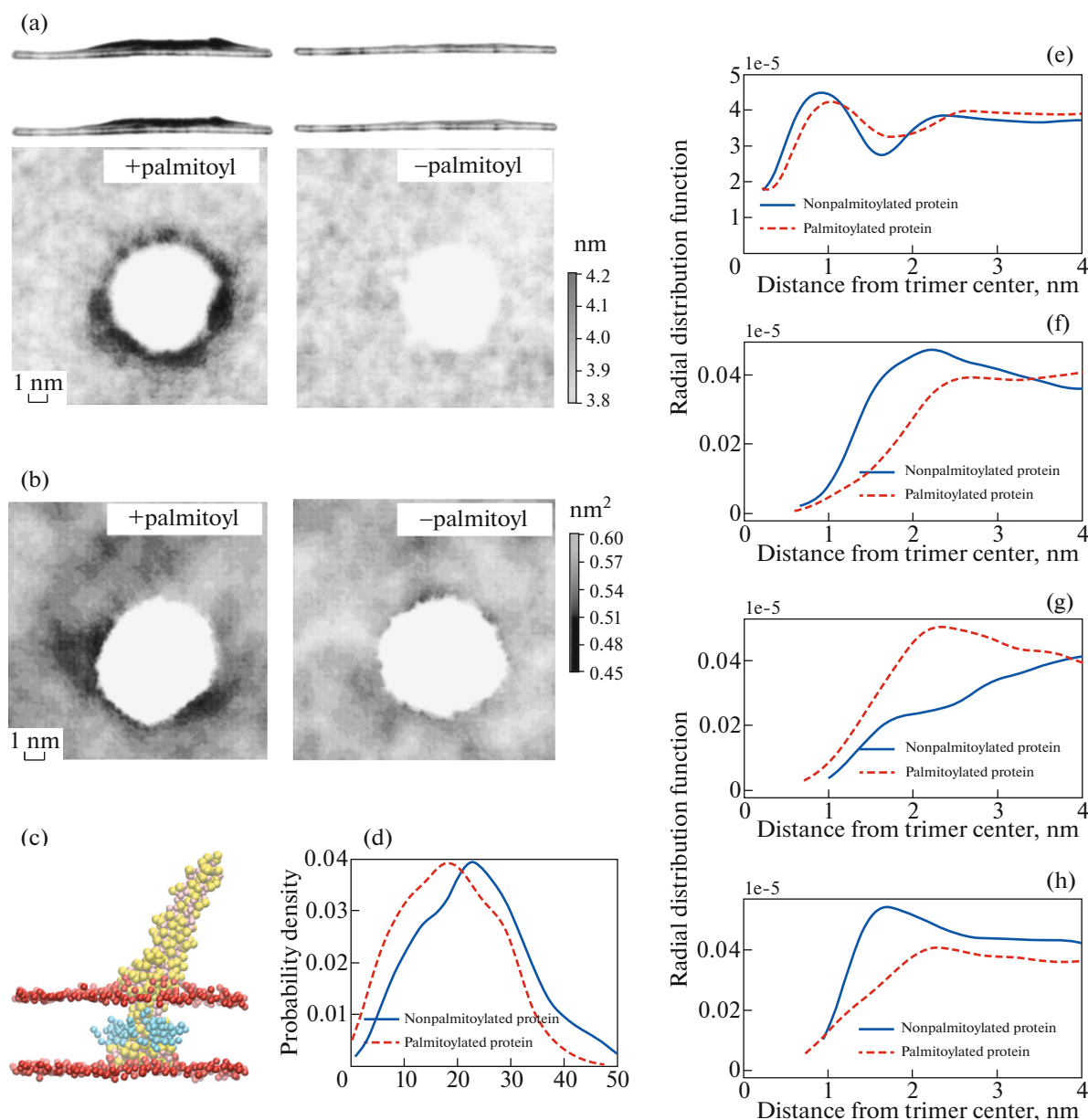


Fig. 2. Coarse-grain trimer modeling in a model lipid membrane. (a) Local bilayer thickness with embedded palmitoylated (left) and nonpalmitoylated (right) trimer. Bilayer shown in the top and lateral view. (b) Averaged local area for a lipid with embedded palmitoylated (left) and nonpalmitoylated (right) trimer. (c) Representative frame from the MD trajectory of palmitoylated trimer (protein particles are represented by grey and yellow spheres and palmitoyl residues, by cyan spheres) with external domain tilted relative to TMD. Only coarse-grain particles corresponding to lipid phosphate groups are indicated within the membrane (red spheres). (d) Distribution of HR2-domain angles relative to TMD. (e–h) Radial distribution functions for cholesterol, POPE, POPC, and POPS, respectively, calculated relative to the TMD axis of mass in the membrane plane.

the conformational conversion of 3-10-helices into α -helices.

Coarse-grain molecular dynamics. To elucidate the effects of the cysteine residues' palmitoylation on the local TMD lipid environment, additional studies of palmitoylated and nonpalmitoylated proteins embedded in a membrane of similar composition were performed using a coarse-grained approximation that allowed increasing the simulation time to 1 μ s.

The local membrane bilayer thickness was calculated for both systems (Fig. 2a). It can be seen that the presence of palmitoyl residues leads to a local thickening and distortion of the membrane around the protein (black area around the white area corresponding to the protein; Fig. 2a). The averaged local area per lipid with the embedded palmitoylated (left) and nonpalmitoylated (right) trimer is shown in Fig. 2b. The lipids around the protein are packed tighter than in the

remaining part of the membrane. In addition, we additionally calculated the radial distribution functions of the lipids present in the membrane relative to the TMD axis of mass in a membrane plane in two systems (Figs. 2e–2h). It can be seen from the obtained results that protein palmitoylation has hardly any effect on the membrane distribution of cholesterol (Fig. 2e) and some other lipids (DPPS, DPPC, DPFE, and PSM, plots not shown), while the radial distribution function values for POPE and POPS (Figs. 2f–2h) near the nonpalmitoylated protein are higher than those near the palmitoylated protein, i.e., the membrane in the TMD region becomes enriched in POPE and POPS. For POPC, the opposite effect is observed consisting in a significantly higher probability of detecting this lipid near a palmitoylated protein compared to a nonpalmitoylated one. Therefore, palmitoylation leads to a significant redistribution of lipid types in a realistic multicomponent bilayer model. Together with the observed membrane thickening and a decrease in the area per lipid near the palmitoylated protein, this may indicate the formation of a raft-like lipid microdomain in its vicinity. These observations are also in good agreement with the palmitoylation effects reported by Charollais and Van Der Goot (2009) [25]: palmitoyls can increase the effective hydrophobic length of the protein TMD by increasing the thickness of the adjacent lipid bilayer and facilitating association with ordered lipids.

In the course of MD simulation, the HR2 domain of the S-protein trimer tilts relative to the TMD (Figs. 2b–2d) in the same way as it does in the case of the all-atom simulation, which correlates well with the maximum angle distribution of approximately 20° and a significant portion of conformations showing the angle between the domains as low as 0° (i.e., a completely “straight” conformation). In addition, the presence of palmitoyl residues slightly reduces the amplitude of the S-protein bend. This may be partly due to the fact that a denser and thicker membrane layer is formed around the TMD protein decreasing its mobility.

The calculated lateral diffusion coefficients for palmitoylated and nonpalmitoylated protein $D_{+\text{palmitoyl}} = (0.0205 \pm 0.0004) \times 10^{-5}$ and $D_{-\text{palmitoyl}} = (0.0025 \pm 0.0001) \times 10^{-5}$ cm²/s indicate that palmitoylation decreases the protein mobility rate in the lateral membrane plate by an order of magnitude. It may be suggested that this decrease facilitates S-protein TMD trimer stabilization.

To summarize, the present study reports the first 3D model of the S-protein TMD and HR-2 domains that would consider cysteine palmitoylation. The protein model was embedded into the membrane of complex composition and optimized. Model stability was evaluated by all-atom and coarse-grain MD simulations. It was shown that the conformational mobility of the HR2-TMD fragment is achieved via bending in

the hinge region located at the boundary between the two domains. We also showed that TMD palmitoylation leads to local changes in the bilayer (its thickening and compaction as well as lipid redistribution) similar to those taking place during raft-like microdomain formation. The model obtained in the present work may be used for interpreting structural data in further studies.

FUNDING

The work was supported by the Russian Foundation for Basic Research (project no. 20-04-60258).

COMPLIANCE WITH ETHICAL STANDARDS

Conflict of interests. The authors declare that they have no conflicts of interest.

Statement on the welfare of humans or animals. This article does not contain any studies involving humans or animals performed by any of the authors.

REFERENCES

1. Letko, M., Marzi, A., and Munster, V., Functional assessment of cell entry and receptor usage for SARS-CoV-2 and other lineage B betacoronaviruses, *Nat. Microbiol.*, 2020, vol. 5, no. 4, pp. 562–569.
2. Walls, A.C., Park, Y.J., Tortorici, M.A., Wall, A., McGuire, A.T., and Velesler, D., Structure, function, and antigenicity of the SARS-CoV-2 spike glycoprotein, *Cell*, 2020, vol. 181, no. 2, pp. 281–292.
3. Turoňová, B., Sikora, M., Schürmann, C., et al., In situ structural analysis of SARS-CoV-2 spike reveals flexibility mediated by three hinges, *Science*, 2020, vol. 370, no. 6513, pp. 203–208.
4. Webb, B. and Sali, A., Protein structure modeling with *MODELLER*, in *Protein Structure Prediction*, Methods in Molecular Biology, vol. 1137, Kihara, D., Ed., New York, NY: Humana, 2014, pp. 239–255.
5. Hakansson-McReynolds, S., Jiang, S., Rong, L., and Caffrey, M., Solution structure of the severe acute respiratory syndrome-coronavirus heptad repeat 2 domain in the prefusion state, *J. Biol. Chem.*, 2006, vol. 281, no. 17, pp. 11965–11971.
6. Fu, Q., Shaik, M.M., Cai, Y., Ghantous, F., Piai, A., Peng, H., Rits-Volloch, S., Liu, Z., Harrison, S.C., Seaman, M.S., Chen, B., and Chou, J.J., Structure of the membrane proximal external region of HIV-1 envelope glycoprotein, *Proc. Natl. Acad. Sci. U.S.A.*, 2018, vol. 115, no. 38, pp. E8892–E8899.
7. Jo, S., Kim, T., Iyer, V.G., and Im, W., CHARMM-GUI: a web-based graphical user interface for CHARMM, *J. Comput. Chem.*, 2008, vol. 29, no. 11, pp. 1859–1865.
8. Woo, H., Park, S.J., Choi, Y.K., Park, T., Tanveer, M., Cao, Y., Kern, N.R., Lee, J., Yeom, M.S., Croll, T.I., Seok, C., and Im, W., Developing a fully glycosylated full-length SARS-CoV-2 spike protein model in a viral membrane, *J. Phys. Chem. B*, 2020, vol. 124, no. 33, pp. 7128–7137.

9. Abraham, M.J., Murtola, T., Schultz, R., Pall, S., Smith, J.C., Hess, B., and Lindahl, E., GROMACS: high performance molecular simulations through multi-level parallelism from laptops to supercomputers, *SoftwareX*, 2015, vols. 1–2, pp. 19–25.
10. Huang, J., Rauscher, S., Nawrocki, G., Ran, T., Feig, M., de Groot, B., Grubmüller, H., and MacKerell, A.J., CHARMM36m: an improved force field for folded and intrinsically disordered proteins, *Nat. Methods*, 2017, vol. 14, no. 1, pp. 71–73.
11. de Jong, D.H., Singh, G., Benett, W.F.D., Arnarez, C., Wassenaar, T.A., Schäfer, L.V., Singh, G., Benett, W.F.D., Arnarez, C., Wassenaar, T.A., Schäfer, L.V., Periole, X., Tieleman, D.P., and Marrink, S.J., Improved parameters for the Martini coarse-grained protein force field, *J. Chem. Theory Comput.*, 2013, vol. 9, no. 1, pp. 687–697.
12. Atsmon-Raz, Y. and Tieleman, D.P., Parameterization of palmitoylated cysteine, farnesylated cysteine, geranylgeranylated cysteine, and myristoylated glycine for the Martini force field, *J. Phys. Chem. B*, 2017, vol. 121, no. 49, pp. 11132–11143.
13. de Jong, D.H., Baoukina, S., Ingolfsson, H.I., and Marrink, S.J., Martini straight: boosting performance using a shorter cutoff and GPUs, *Comput. Phys. Commun.*, 2016, vol. 199, pp. 1–7.
14. Gapsys, V., de Groot, B.L., and Briones, R., Computational analysis of local membrane properties, *J. Comput.-Aided Mol. Des.*, 2013, vol. 27, no. 10, pp. 845–858.
15. Dev, J., Park, D., Fu, Q., Chen, J., Ha, H.J., Ghan-tous, F., Herrmann, T., Chang, W., Liu, Z., Frey, G., Seaman, M.S., Chen, B., and Chou, J.J., Structural basis for membrane anchoring of HIV-1 envelope spike, *Science*, 2016, vol. 353, no. 6295, pp. 172–175.
16. Chiliveri, S.C., Louis, J.M., Ghirlando, R., Baber, J.L., and Bax, A., Tilted, uninterrupted, monomeric HIV-1 gp41 transmembrane helix from residual dipolar couplings, *J. Am. Chem. Soc.*, 2018, vol. 140, no. 1, pp. 34–37.
17. Mahajan, M. and Bhattacharjya, S., Solution structure of pre transmembrane domain. Worldwide Protein Data Bank, 2014.
<https://doi.org/10.2210/pdb2run/pdb>
18. Veit, M., Palmitoylation of virus proteins, *Biol. Cell*, 2012, vol. 104, no. 9, pp. 493–515.
19. Petit, C.M., Chouljenko, V.N., Iyer, A., Colgrove, R., Farzan, M., Knipe, D.M., and Kousoulas, K.G., Palmitoylation of the cysteine-rich endodomain of the SARS-coronavirus spike glycoprotein is important for spike-mediated cell fusion, *Virology*, 2007, vol. 360, no. 2, pp. 264–274.
20. Best, R.B., Zhu, X., Shim, J., Lopes, P.E.M., Mittal, J., Feig, M., and MacKerell, A.D., Optimization of the additive CHARMM all-atom protein force field targeting improved sampling of the backbone ϕ , ψ and side-chain χ_1 and χ_2 dihedral angles, *J. Chem. Theory Comput.*, 2012, vol. 8, no. 9, pp. 3257–3273.
21. Krogh, A., Larsson, B., von Heijine, G., and Sonnhammer, E.L.L., Predicting transmembrane protein topology with a hidden Markov model: application to complete genomes, *J. Mol. Biol.*, 2001, vol. 305, no. 3, pp. 567–580.
22. Serebryakova, M.V., Kordyukova, L.V., Baratova, L.A., and Markushin, S.G., Mass spectrometric sequencing and acylation character analysis of C-terminal anchoring segment from influenza A hemagglutinin, *Eur. J. Mass Spectrom.*, 2006, vol. 12, no. 1, pp. 51–62.
23. Fu, Q. and Chou, J.J., A trimeric hydrophobic zipper mediates the intramembrane assembly of SARS-CoV-2 spike, *bioRxiv*, 2021.
<https://doi.org/10.1021/jacs.1c02394>
24. Thorp, E.B., Boscarino, J.A., Logan, H.L., Goletz, J.T., and Gallagher, T.M., Palmitoylations on murine coronavirus spike proteins are essential for virion assembly and infectivity, *J. Virol.*, 2006, vol. 80, no. 3, pp. 1280–1289.
25. Charollais, J. and van der Goot, F.G., Palmitoylation of membrane proteins (review), *Mol. Membr. Biol.*, 2009, vol. 26, no. 1, pp. 55–66.

Translated by E. Martynova